GDCh Research Article Angewandte International Edition Chemie www.angewandte.org

How to cite: *Angew. Chem. Int. Ed.* **2025**, e202503090
doi.org/10.1002/anie.202503090

Porous Materials

Turing-Structured Covalent Organic Framework Membranes for Fast and Precise Peptide Separations

Bingjie Gao, Youxin Gong, Zhe Zhang, Qinghua Liu, Congcong Yin, Mingjie Wei, and Yong Wang**

Abstract: Turing structures have emerged as promising features for separation membranes, enabling significantly enhanced water permeation due to their ultra-permeable internal cavities. So far, Turing structures are constrained by the highly cross-linked and heterogeneous porosities, impeding them from the application of molecular separations requiring loose but regular pore structures. This work reports a covalent organic frameworks (COFs) membrane with nanoscale striped Turing structures for fast and precise molecular separations. Porous and hydrophilic modulation layers based on metal-polyphenol chemistry are constructed on polymeric substrates, which are capable of enhancing the uptake and controlled release of the activator of amines during synthesis. The appropriately reduced diffusion rate triggers the phenomenon of "local activation and lateral inhibition" arising from thermodynamic instability, creating Turing structures with externally striped and internally cavitated architectures. The Turing-type COF membranes exhibit a water permeance of 45.0 L m^{-2} h^{-1} bar^{-1}, which is approximately 13 times greater than the non-Turing membranes, and an ultrahigh selectivity of up to 638 for two model peptides. This work demonstrates the feasibility that Turing structures with ultra-permeable internal cavities can be created in COF membranes and underscores their superiority in molecular separations, including but not limited to high-value pharmaceuticals.

Introduction

In 1952, Alan Turing's pioneering paper, "The chemical basis of morphogenesis," predicted a chemical reaction-diffusion model in which a couple of activators and inhibitors can, to some extent, react and diffuse to create spatiotemporal stationary patterns.[1] This has served as a basic model in biology and chemistry, which provides theoretical insights into how heterogeneous patterns such as stripes, spots, and spirals may arise spontaneously out of a homogeneous state.[2] Later, experimental evidence of stationary Turing states was observed in the reactions of chlorite–iodide–malonic acid[3,4] and the Belousov–Zhabotinsky,[5] respectively, and a series of spatial Turing structures have been studied in biological and chemical systems.[3,6–8] The first example of Turing-type separation membrane was reported by Zhang and co-workers,[9] who created polyamide nanofiltration membranes with nanoscale bubble and tube structures, enabling excellent water-salt separation performances. The creation of Turing structures is necessary for separation membranes, because of the existence of abundant cavities within the internal structures.[9] The nanoscale cavities are amenable to enhanced water permeation,[10–13] which are generally recognized as the key feature of Turing-type membranes. This provides a straightforward means by which permeability and selectivity can be enhanced simultaneously, circumventing the trade-off effect that has been observed in most scenarios.

Membranes with the Turing patterns have been frequently observed in polyamide nanofiltration membranes,[14–17] which are created by interfacial polymerization based on a reaction-diffusion process far from thermodynamic equilibrium.[18,19] Typically, the amines dissolving in water serve as the activator, while the acyl chlorides dissolving in an organic solvent work as the inhibitor. The activator first reacts with the inhibitor at the organic phase and further diffuses into the deep region to accomplish the polymerization reaction, so that a cross-linked network membrane is formed at the interface. To create Turing patterns, there must be an appropriate difference between the diffusion coefficient of the activator and the inhibitor.[9] Considerable effort has been made to achieve the difference of the diffusion coefficient, such as the incorporation of modulators[20–23] and the construction of intermediate layer.[24–26] Those membranes exhibit markedly enhanced water transport properties without compromising solute rejections. Thus far, Turing-type polyamide membranes are limited to the application of ion separations, as the highly cross-linked membranes possess high water-ion or ion-ion

[*] B. Gao, Y. Gong, Q. Liu, Prof. M. Wei, Prof. Y. Wang
State Key Laboratory of Materials-Oriented Chemical Engineering, and College of Chemical Engineering, Nanjing Tech University, Nanjing, Jiangsu 211816, P.R. China
E-mail: yongwang@seu.edu.cn

Dr. Z. Zhang
School of Environmental Science and Engineering, Nanjing Tech University, Nanjing, Jiangsu 211816, P.R. China
E-mail: zhangzhe@njtech.edu.cn

Dr. C. Yin, Prof. Y. Wang
School of Energy and Environment, Southeast University, Nanjing, Jiangsu 210096, P.R. China

Additional supporting information can be found online in the Supporting Information section

selectivities but poor selectivity to small organic molecules.[27] The latter requires relatively loose membrane structures for molecular separation. Furthermore, the inherent fast and stochastic cross-linking process of interfacial polymerization makes it difficult to accurately control the pore structures,[28] leading to inadequate separation precision.

Two-dimensional covalent organic frameworks (COFs) are porous and crystalline framework materials, in which two building blocks are covalently linked into extended architectures through reticular chemistry.[29–31] Unlike the instantaneous and irreversible reactions forming heterogeneous microporosity, the reversible reaction of COFs allows self-repairing processes to obtain crystalline structures with regular pores. The homogeneous open pores with sub-2-nm apertures are promising alternatives to prepare loose nanofiltration membranes for precise molecular separations.[32,33] It can be envisioned that COF membranes with Turing structures could potentially exhibit fast and precise transport properties, by leveraging their ultra-permeable cavities and homogeneous porosities. However, compared to polyamide membranes, the relatively low reaction rate and the indistinguishable diffusion coefficient of monomers could not reach the threshold to trigger thermodynamic instability required for creating Turing structures.[34] It remains a formidable challenge to create Turing-type COF membranes, but is of fundamental significance to both scientific and practical interests.

Herein, we report a Turing-type COF membrane prepared by the modulation of metal-polyphenol chemistry (Figure 1). Exemplified by the complex of tannic acid and $FeCl_3$ (TA–Fe), it was deposited onto substrates. Due to the porous and hydrophilic nature, the TA–Fe layer can slow down the diffusion rate of the activator via the enhanced uptake and controlled release. The resultant membranes possess striped Turing structures with abundant internal cavities, and these architectures can be well tuned by changing the concentration of the activator during synthesis. The resultant membranes exhibit fast water permeation, which is ~13 times greater than the membrane without Turing structure. Furthermore, the membrane has the ability to separate high-value pharmaceutical, for example, peptides with high precision, demonstrating its great potential in loose nanofiltration applications.

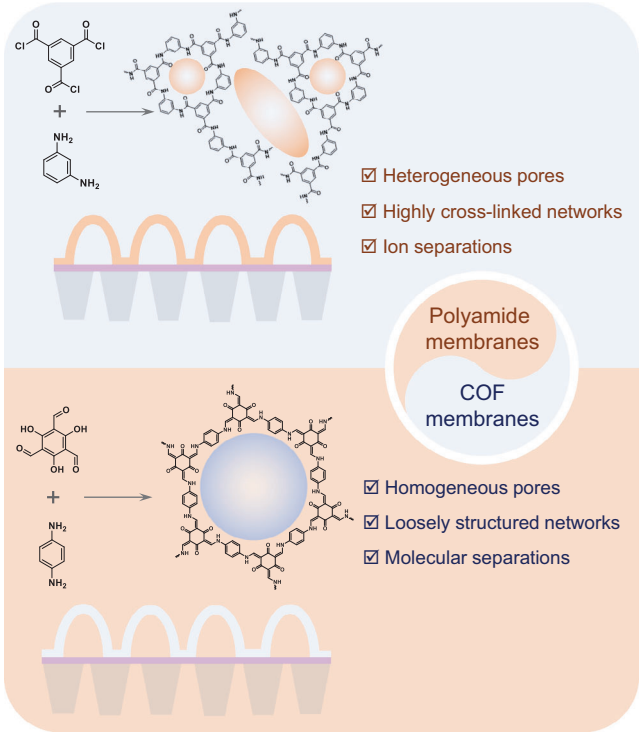

Figure 1. Schematic diagram of the comparison of the Turing structures in conventional polyamide and COF membranes. Conventional Turing-type polyamide membranes possess heterogeneous pores and highly cross-linked networks, falling in the range of tight nanofiltration used for ion separations. Turing-type COF membranes feature homogeneous pores and loosely structured networks, which can be used in molecular separations requiring loose nanofiltration.

Results and Discussion

Microstructures and Properties of Membranes

We choose a β-ketoenamine-linked COF, TpPa, as the model to study the creation of Turing-type membranes, which is based on the following considerations.[35] TpPa possesses a simple and clear framework structure with a sub-2-nm aperture, which can be synthesized under ambient conditions without complex monomers. Moreover, the β-ketoenamine linkage has been proven to be chemically stable, which is amenable to various separation applications. Conventional TpPa membranes can be synthesized through a polycondensation reaction of 1,3,5-triformylphloroglucinol (Tp) and *p*-phenyleneamine (Pa) on porous substrates (Figure S1). Typically, the aldehyde monomer Tp is dissolved in an organic solvent serving as the inhibitor, while the amine monomer Pa is dissolved in water working as the activator. Due to the inappropriate differences between the diffusion coefficients of the inhibitor and the activator, those membranes are of not Turing structures. We used metal-polyphenol chemistry to deposit a modulation layer on a porous substrate to slow down the diffusion rate of the activator. The reduced diffusion rate would lead to the phenomenon of "local activation and lateral inhibition" arising from thermodynamic instability, which creates the Turing patterns. Exemplified here by depositing a complex of TA-Fe (Figures S2, S3), they are reported to be a robust network with high hydrophilicity and porosity.[36] Their good affinity toward organic amines is capable of controlling the diffusion rate.

From scanning electron microscopy (SEM) images (Figure S4), the TA-Fe complex was uniformly deposited on the polyacrylonitrile (PAN) porous substrate, and the as-deposited substrate is named TA–Fe–PAN. TpPa membranes synthesized from the TA–Fe–PAN substrate exhibited a heterogeneous morphology with striped Turing structures (Figures 2a and S5). Those stripes were interconnected into labyrinthine networks, and the diameters of the stripes were 46 nm. No defect can be seen on the membrane surface. This membrane with striped Turing structures is noted as Turing-type TpPa membrane. For comparison, TpPa membranes without Turing structures were prepared on a

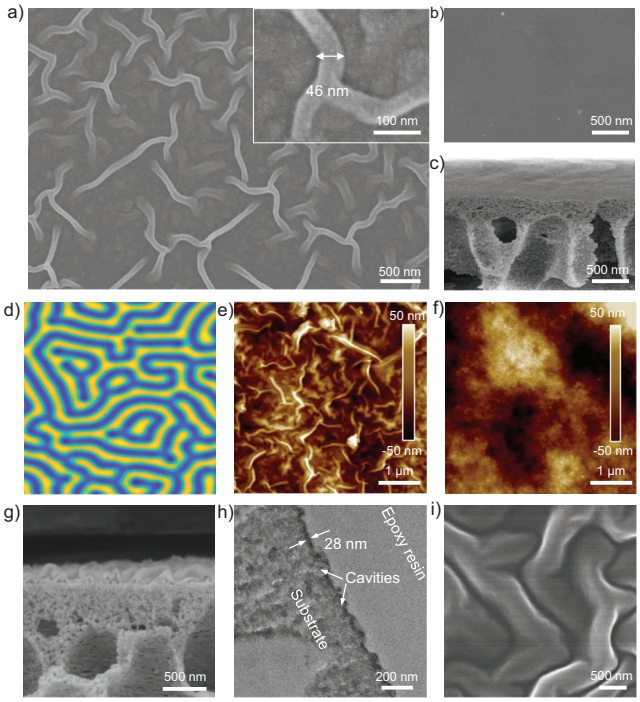

Figure 2. Microstructures of membranes. a) The surface SEM image of the Turing-type TpPa membrane. Inset shows the corresponding high-magnification SEM image. Surface b) and cross-sectional c) SEM images of the TpPa membrane. d) The schematic diagram of the striped Turing patterns generated by MATLAB. AFM images of the Turing-type TpPa e) and TpPa f) membranes. The cross-sectional SEM g) and TEM h) images of the Turing-type TpPa membrane. i) The SEM image of the rear surface of the Turing-type TpPa membrane.

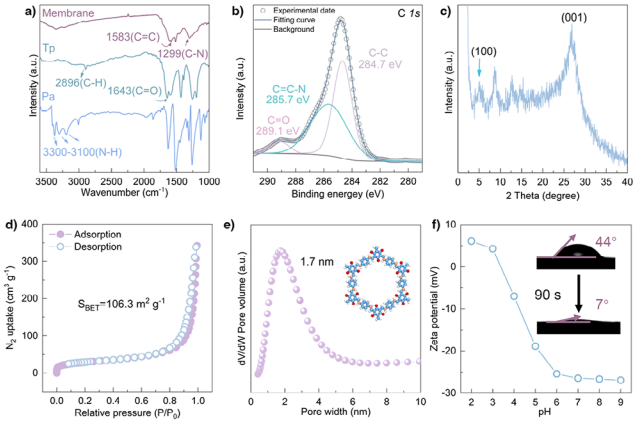

Figure 3. Physicochemical properties of the Turing-type TpPa membrane. a) FTIR spectra. b) XPS spectra. c) XRD pattern. d) Nitrogen sorption isotherms. e) The corresponding pore size distribution. Inset shows the molecular structure of TpPa. f) The Zeta potential. Inset shows the water contact angles.

neat PAN substrate, which termed as TpPa membrane. The TpPa membrane displayed a smooth surface with a low thickness of 20 nm (Figures 2b,c and S6), which is different than that of Turing-type TpPa membrane. In addition, the appearance of the Turing-type TpPa membrane was in black color (Figure S7), while the TpPa membrane was bright green, probably due to the scattered reflection caused by the rough and heterogeneous surface. To further reveal the Turing structures, we used MATLAB to generate a schematic diagram (Figure 2d), which agreed with the SEM observation. Atomic force microscopy (AFM) images also confirmed the formation of striped Turing structures compared to the relatively smooth surface of the TpPa membrane (Figure 2e,f). The cross-sectional SEM image provided the internal information of the striped Turing structures (Figure 2g). Underneath the wrinkled nanofilms, a large number of inner cavities can be observed. Moreover, the cross-sectional transmission electron microscopy (TEM) further revealed the inner cavities and an ultrathin thickness of the wrinkled nanofilm was 28 nm (Figure 2h). In sharp contrast, the TpPa membrane exhibited a flat rather than a wrinkled nanofilm. The wrinkled nanofilm can be released from the substrate by etching away the TA-Fe layer so as to uncover the rear surface of the wrinkled nanofilm. As shown in Figure 2i, the rear surface displayed a very similar structure compared to the upper surface without any defects, indicating the consistency of both external and internal structures of the striped Turing structures. For the TpPa membrane, the rear surface showed a relatively flat structure with some visible defects (Figure S8).

Fourier-transform infrared spectroscopy (FTIR) spectra confirmed the successful synthesis of TpPa (Figure 3a). The vibrational band at 1643 cm^{-1} (C═O), 2896 cm^{-1} (C─H) and 3300–3100 cm^{-1} (N-H) assigned to Tp and Pa monomers were absent in the spectrum of TpPa. Although the vibrational bands at 1583 cm^{-1} (C═C) and 1299 cm^{-1} (C─N) of the β-ketoenamine linkage appeared.[35] X-ray photoelectron spectroscopy (XPS) spectra also proven the chemical structures of TpPa, as the characteristic peaks of C─C, C═C─N and C═O belonging to the backbone of TpPa can be detected (Figure 3b). The X-ray diffraction (XRD) pattern showed two major diffraction peaks located at ~5° and 26°, respectively, which can be ascribed to the (100) and (001) planes, indicating its crystalline structures (Figure 3c).[35] Notably, the peaks were not seemingly intense, as the membrane sample was used during the measurement, while they are comparable to those reported in other works.[34,37] Nitrogen sorption measurement was conducted to obtain the information on porosities. The Turing-type TpPa membrane exhibited a relatively high Brunauer–Emmett–Teller (BET) surface area of 106.3 m^2 g^{-1} (Figure 3d), with a pore size of 1.7 nm (Figure 3e). Due to the intrinsic electronegativity of the β-ketoenamine linkage,[38] the Turing-type TpPa membrane possessed a negatively charged surface over a broad pH range (Figure 3f). Furthermore, the negatively charged surface with abundant wrinkles accounts for the excellent water wettability, as the water droplet can almost spread out the membrane surface within 90 s.

Mechanistic Insights into the Formation of Turing Structures

To understand what important role the TA-Fe layer played, quartz crystal microbalance with dissipation (QCM-D) measurement was conducted to analyze the adsorption and

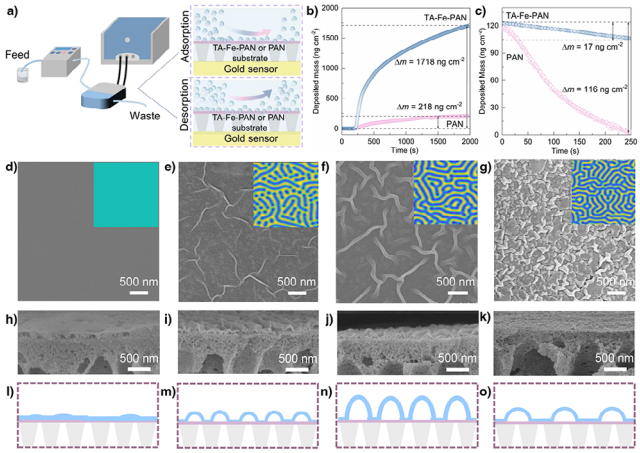

Figure 4. The formation of striped Turing structures. a) Schematic diagram of QCM-D. b) QCM-D absorption test of Pa monomers on different substrates. c) QCM-D desorption test of Pa monomers on different substrates. SEM images of surface d)–g), cross section h)–k), and corresponding schematic diagrams l)–o) of the Turing-type TpPa membranes prepared from different Pa concentrations of 5 mM (d), (h), (l), 14 mM (e), (i), (m), 23 mM (f), (j), (n), 32 mM (g), (k), (o). Insets in (d–g) show the schematic diagram of the striped Turing patterns generated by MATLAB.

desorption of the Pa monomer by different substrates (Figure 4a). As shown in Figure 4b, the TA–Fe–PAN substrate exhibited a high adsorption capacity of 1718 ng cm^{-2}, which is approximately eight times greater than that of the PAN substrate (218 ng cm^{-2}). The highly porous and hydrophilic networks of the TA–Fe layer may account for the strong adsorption of Pa monomers. For desorption, the capacity of the TA–Fe–PAN substrate was 17 ng cm^{-2}, after a duration of 250 s (Figure 4c). In contrast, the PAN substrate showed a desorption capacity of 116 ng cm^{-2}, which is nearly seven times higher than that of the TA–Fe–PAN substrate. The Above findings indicated that the TA–Fe layer enhanced the uptake and controlled release of Pa monomers, giving rise to a much reduced diffusion rate of the activator than that of the inhibitor. This appropriate difference would allow the occurrence of thermodynamic instability to trigger the creation of Turing patterns.

We further studied whether or to what extent the monomer concentration could influence the formation of Turing patterns. A series of Turing-type TpPa membranes were prepared with different Pa concentrations of 5, 14, 23, and 32 mM, respectively. The concentration ratio of Pa and Tp monomers was set to ~3. From surface SEM images (Figure 4d–g), at a lower concentration of 5 mM, the surface was relatively smooth without obvious Turing patterns. With increasing the concentration to 14 mM, a small number of Turing patterns with slim stripes began to emerge. These slim stripes became larger when the concentration reached 23 mM. Further increasing the concentration to 32 mM, the membrane surface displayed crowded and short stripes, which is different compared to the membranes prepared from lower concentrations. In addition, the corresponding AFM images and the schematic diagrams also supported the variation trend of the Turing patterns with different Pa concentrations (Figure S9). We then checked the cross sections of those Turing-type TpPa membranes to reveal the changes of their internal structures (Figure 4h–k). The membrane prepared from the Pa concentration of 5 mM did not show wrinkled nanofilms, but some voids between the nanofilm and the underneath TA-Fe layer. On the contrary, the wrinkled nanofilms with abundant internal cavities can be clearly observed in the scenario where higher Pa concentrations were used. Notably, these cavities were geometrically structured in different fashions (Figure 4l–o). The membrane prepared from the Pa concentration of 14 mM exhibited similar structures but different height of the cavities, compared to the membrane prepared from the concentration of 23 mM. Although the membrane prepared from the concentration of 32 mM showed wide cavities with similar height compared to the membrane prepared from the concentration of 14 mM. To understand how the concentration ratio of Pa and Tp could affect the creation of Turing structures, we prepared the membranes with the same Pa concentrations used above, but a fixed Tp concentration of 8 mM. From SEM images (Figure S10), all these membranes exhibited striped Turing patterns, while a better structure seem to be the membrane prepared from the Pa concentration of 23 mM. Additionally, we investigated the universality of the metal-polyphenol chemistry on the creation of Turing structures. Metal sources of $CuCl_2$, $CaCl_2$, and $ZnCl_2$ were used to initiate the complexation with TA, respectively, to prepare different modulation layers on PAN substrates. From SEM images (Figure S11), the surfaces were relatively flat, similar to that of the TA-Fe layer. The as-synthesized membranes also exhibited a black color in appearance (Figure S12), and striped Turing structures can be clearly observed (Figure S13), indicating the applicability of metal-polyphenol chemistry for creating Turing structures. Note that, for other COFs, the conditions for triggering the formation of Turing structures need to be explored. We also prepared a TA-modified PAN substrate without adding metal ions, and the surface did not change compared to the neat substrate (Figure S14). Using this substrate to grow TpPa layer, no Turing structure can be observed (Figure S15). Notably, TA can be solely used to modulate the growth of TpPa.[34] Above findings indicated that the Turing patterns can be created by the modulation of the TA-Fe layers via the enhanced uptake and controlled release of Pa monomers during membrane synthesis. Moreover, the concentration of Pa monomers plays a vital role in creating the Turing patterns, and a better structure can be obtained from the Pa concentration of 23 mM.

Water Transport and Molecular Separation Performances

To reveal the structure-performance relationship between the Turing structures and the nanofiltration performances, we correlated the external and internal structures of the Turing patterns (Figure 5a). To quantify the feature of the Turing structures, specific length of stripes and aspect ratio of stripes were defined respectively.[39] The former refers to the ratio of stripe length with a certain area of 1 μm^2, and the latter is an aspect ratio of the height with the half width of the

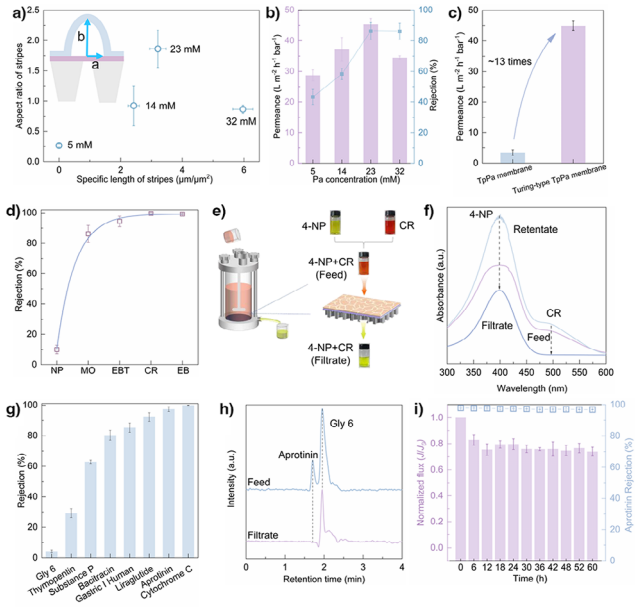

Figure 5. Nanofiltration performances of membranes. a) The correlation of external and internal features of the striped Turing structures. b) Changes of water permeance and MO rejection with different Pa concentrations. c) Comparison on water permeance of different membranes. d) Rejection characteristics of the Turing-type TpPa membrane using different dyes. The selective separation of a mixture of CR and 4-NP: the schematic diagram e) and the corresponding UV-vis spectra f). g) Rejection characteristics of different peptides. h) The high-performance liquid chromatography spectra of the feed and the filtrate of Gly 6 and aprotinin. i) Separation stability test of the aprotinin. Error bars represent the standard deviation of three independent experiments.

cavity (b/a) Taken together, the optimal structure seems to be the membrane prepared from the Pa concentration of 23 mM, as the length of the strip and the volume of the cavity can be maximized simultaneously. The nanofiltration performances was evaluated using methyl orange (MO) as the probe, the size of which is ~1.5 nm,[40] slightly smaller but very close to the pore size of the Turing-type TpPa membrane (Figure 5b). When the Pa concentrations increased from 5 to 23 mM, the water permeance and MO rejection continue to rise. This is well in line with the trend of the Turing structures as mentioned above. The enlarge of both the strips and cavities leads to the formation of highly permeable sites, which accounts for enhanced water permeance. Furthermore, the increased Pa concentration favored the formation of defect-free membranes because of the improved self-repairing process under higher monomer concentrations.[41] With further increasing the Pa concentration to 32 mM, the MO rejection remained unchanged, while the water permeance declined. This phenomenon also agreed with the changes of the Turing structures. Ultimately, the optimal nanofiltration performance can be obtained with a high water permeance of 45.0 L m^{-2} h^{-1} bar^{-1}, coupled with a MO rejection of 86.3%. Importantly, compared with the TpPa membrane with a water permeance of 3.4 L m^{-2} h^{-1} bar^{-1}, the Turing-type TpPa membrane exhibited ~13 times greater enhancement of water permeance (Figure 5c). Furthermore, the MO rejection of the Turing-type TpPa membrane was better than that of the TpPa membrane (83.5%). It should be noted that, in addition to the ultra-permeable sites, the TA–Fe layer favors the unimpeded water permeation. Despite the thin thickness of the TpPa membranes, its water permeance was very low. This can be explained by the intrusion of the TpPa layer into the substrate, resulting in increased resistance for water transport.[42] The TA–Fe layer can well tackle such a problem, as it works as a continuous scaffold to prevent the TpPa layer from the intrusion, which has been observed in the formation of polyamide membranes.[43] Moreover, the porous and hydrophilic TA–Fe layer can serve as a gutter layer to better transport water molecules by providing abundant shortcuts from the TpPa layer to the pore openings of the PAN substrate.[44] Notably, the Turing structures were well maintained after the pressurized filtration, as well as the soaking by different solvents (Figures S16, S17).

We investigated the rejection characteristic of the Turing-type TpPa membrane using dye molecules with different sizes. The membrane exhibited high rejections to MO (1.5 nm), eriochrome black T (EBT, 1.6 nm), Congo red (CR, 2.5 nm), and Evans blue (EB, 2.8 nm), while showed low rejection to *p*-nitrophenol (4-NP, 0.7 nm) with a much smaller molecular size (Figure 5d). The size exclusion and charge interaction govern the separation process, due to the inherently regular pores and negatively charged surface of the Turing-type TpPa membranes. Note that the TA-Fe layer did not exhibit obvious rejection of these dyes, indicating that the COF layer accounts for the rejection exclusively (Figure S18). The precise separation capability was demonstrated by selectively separating a mixture of CR and 4-NP with an equal concentration of 50 ppm (Figure 5e). The Turing-type TpPa membrane almost completely rejected CR molecules while allowing 4-NP molecules to pass through the membrane freely, as the absorbance belonging to CR cannot be detected in the spectrum of the filtrate (Figure 5f). In addition, we evaluated the nanofiltration performances of the Turing-type TpPa membranes prepared from different concentration ratios of Pa and Tp. The variation trend of water permeance and MO rejection was inconsistent with that of their structures (Figure S19). The Turing-type TpPa membranes prepared from other metal-polyphenol layers exhibited higher water permeance than that of the TpPa membrane, while maintaining an almost unchanged MO rejection (Figure S20).

Considering the excellent molecular sieving capability, we thus studied the applicability of the Turing-type TpPa membranes in the separation of peptides. The peptides are high-value pharmaceuticals,[45,46] that require energy-intensive and time-consuming processes, including crystallization and chromatography. Membrane separation provides an energy-efficient way, but precise molecular separation processes rely on the accurate control of the membrane pores, in which the conventional polymeric membranes are not doing so well. We evaluated the rejection characteristic of a series of peptides with different molecular weights (Figure S21), including Gly 6 (M_W: 360 Da), thymopentin (M_W: 679 Da), substance P (M_W: 1347 Da), bacitracin (M_W: 1421 Da), gastrin I human (M_W: 2098 Da), liraglutide (M_W: 3751 Da), aprotinin

(M_W: 6512 Da), and cytochrome C (M_W: 12 588 Da). As shown in Figure 5g, the rejections of liraglutide, aprotinin, and cytochrome C were higher than 90%, and the membrane exhibited moderate rejections of substance P, bacitracin and gastrin I human. Lower rejections can be obtained when Gly 6 and thymopentin are used. Therefore, the Turing-type TpPa membrane possessed a gradient rejection characteristic for peptides with different molecular weights. Above results are also in accordance with that of the retention test, as the molecular weight cut off was measured to be 2468 Da (Figure S22). We then selected a pair of peptides containing Gly 6 and aprotinin to evaluate the potential separation capability in practical applications, as the Gly 6 is typically used as the starting materials to synthesize peptides with higher molecular weights[47] As shown in Figure 5h, after the nanofiltration, the peak in the filtrate belonging to the aprotinin was not detected, while the peak of Gly 6 in the filtrate remained almost unchanged. Based on the spectra, the rejections of aprotinin and Gly 6 were 99.9% and 36.2%, and thus the separation factor of Gly 6 and aprotinin can be calculated to be 638. The slightly enhanced rejection of Gly 6 can be ascribed to the entanglement of its long chain with aprotinin in mixture solutions, and a small part of Gly 6 would be rejected along with aprotinin. Moreover, the molecular shape and size also influence the rejection of peptides. For instance, despite the similar molecular weight, Gly 6 can easily pass through the membrane, because of its long-and-thin molecular chains, compared to that of MO. This separation performance is better than many other membranes used for peptide separations reported in literature (Table S1), demonstrating the excellent molecular sieving capability of the Turing-type TpPa membrane. In addition, the Turing-type TpPa membrane maintained almost unchanged rejection of aprotinin over a long period of time (60 h), while a slight decline in permeance is due to the membrane fouling by the peptides.

Conclusion

In summary, we reported TpPa membranes with nanoscale striped Turing structures constructed on a TA–Fe modulation layer. It was found that the porous and hydrophilic TA–Fe layer enhanced the uptake and controlled release of the activator, triggering the thermodynamic instability. This can significantly reduce the diffusion of the activator toward the organic phase during synthesis, resulting in the creation of Turing structures base on the phenomenon of "local activation and lateral inhibition." The Turing structures were nanoscale strips in the external structures, and possessed abundant cavities in the internal structures. Such an architecture favored the formation of ultra-permeable sites, giving rise to significantly enhanced water permeance, which is ~13 times higher than that of the membrane without Turing structures. Furthermore, the Turing-type TpPa membranes were capable of sieving high-value pharmaceuticals, such as peptides with different molecular weights. This works provided a direct way to create Turing-structures on COF membranes, which demonstrates great potential in the loose nanofiltration applications requiring fast and precise molecular separations.

Acknowledgements

This work was supported by the National Natural Science Foundation of China (U24A2083, 22308147).

Conflict of Interests

The authors declare no conflict of interest.

Data Availability Statement

The data that support the findings of this study are available from the corresponding author upon reasonable request.

Keywords: Covalent organic frameworks (COFs) · Nanofiltration · Polypeptide separation · Turing structures

[1] A. M. Turing, *Philos. Trans. R. Soc. Lond. B Biol. Sci.* **1952**, *237*, 37–72.
[2] A. Gierer, H. Meinhardt, *Kybernetik* **1972**, *12*, 30–39.
[3] V. Castets, E. Dulos, J. Boissonade, P. De Kepper, *Phys. Rev. Lett.* **1990**, *64*, 2953–2956.
[4] Q. Ouyang, H. L. Swinney, *Nature* **1991**, *352*, 610–612.
[5] V. K. Vanag, I. R. Epstein, *Phys. Rev. Lett.* **2001**, *87*, 228301.
[6] J. Gu, L. Li, Y. Xie, B. Chen, F. Tian, Y. Wang, J. Zhong, J. Shen, J. Lu, *Nat. Commun.* **2023**, *14*, 5389.
[7] Y. Zhang, N. Zhang, Y. Liu, Y. Chen, H. Huang, W. Wang, X. Xu, Y. Li, F. Fan, J. Ye, Z. Li, Z. Zou, *Nat. Commun.* **2022**, *13*, 2942.
[8] D. J. Finney, *Nature* **1959**, *183*, 1766–1766.
[9] Z. Tan, S. Chen, X. Peng, L. Zhang, C. Gao, *Science* **2018**, *360*, 518–521.
[10] C. Zhao, Y. Zhang, Y. Jia, B. Li, W. Tang, C. Shang, R. Mo, P. Li, S. Liu, S. Zhang, *Nat. Commun.* **2023**, *14*, 1112.
[11] L. Zhang, R. Li, S. Zheng, H. Zhu, M. Cao, M. Li, Y. Hu, L. Long, H. Feng, C. Y. Tang, *Nat. Commun.* **2024**, *15*, 9738.
[12] Q. Gan, Y. Hu, C. Wu, Z. Yang, L. E. Peng, C. Y. Tang, *Environ. Sci. Technol.* **2024**, *58*, 20812–20829.
[13] Z. Wang, Z. Wang, S. Lin, H. Jin, S. Gao, Y. Zhu, J. Jin, *Nat. Commun.* **2018**, *9*, 2004.
[14] C. Jiao, X. Song, X. Zhang, L. Sun, H. Jiang, *ACS Appl. Mater. Interfaces* **2021**, *13*, 18380–18388.
[15] N. Song, X. Xie, D. Chen, G. Li, H. Dong, L. Yu, L. Dong, *J. Membr. Sci.* **2021**, *621*, 118985.
[16] F. Xiao, M. Cao, Y. Chen, *Desalination*, **2022**, *544*, 116146.
[17] X.-L. Zhang, P.-P. Yang, Y.-R. Zheng, Y. Duan, S.-J. Hu, T. Ma, F.-Y. Gao, Z.-Z. Niu, Z.-Z. Wu, S. Qin, L.-P. Chi, X. Yu, R. Wu, C. Gu, C.-M. Wang, X.-S. Zheng, X. Zheng, J.-F. Zhu, M.-R. Gao, *Angew. Chem. Int. Ed.* **2021**, *60*, 6553–6560.
[18] E. L. Wittbecker, P. W. Morgan, *J. Polym. Sci.* **1959**, *40*, 289–297.
[19] P. W. Morgan, S. L. Kwolek, *J. Polym. Sci.* **1959**, *40*, 299–327.
[20] B. Yuan, Y. Zhang, P. Qi, D. Yang, P. Hu, S. Zhao, K. Zhang, X. Zhang, M. You, J. Cui, J. Jiang, X. Lou, Q. J. Niu, *Nat. Commun.* **2024**, *15*, 471.
[21] L. Fang, H. Xu, S. Qiu, T. Ye, T. Wang, J. Shang, C. Gu, S. Kitagawa, L. Li, *Angew. Chem. Int. Ed.* **2025**, *64*, e202423220.
[22] L. Zhou, X. Li, K. Cao, Z. Jia, H. Long, Y. Li, G. Tao, N. Liu, J. Zhang, L. Ma, *Adv. Funct. Mater.* **2022**, *32*, 2108178.
[23] C. Tian, D. Lei, Y. Qian, X.-Y. Kong, Z. Liu, *Sep. Purif. Technol.* **2025**, *358*, 130335.

[24] Z. Wang, L. Bai, J. Wang, H. Liang, G. Li, *J. Membr. Sci.* **2023**, *683*, 121819.
[25] X. Luo, M. Zhang, Y. Hu, Y. Xu, H. Zhou, Z. Xu, Y. Hao, S. Chen, S. Chen, Y. Luo, Y. Lin, J. Zhao, *Science.* **2024**, *385*, 647–651.
[26] J. Wu, C. Yuan, T. Li, Z. Yuan, H. Zhang, X. Li, *J. Am. Chem. Soc.* **2021**, *143*, 13135–13144.
[27] R. Epsztein, R. M. DuChanois, C. L. Ritt, A. Noy, M. Elimelech, *Nat. Nanotechnol.* **2020**, *15*, 426–436.
[28] Z. Jiang, R. Dong, A. M. Evans, N. Biere, M. A. Ebrahim, S. Li, D. Anselmetti, W. R. Dichtel, A. G. Livingston, *Nature*. **2022**, *609*, 58–64.
[29] C. S. Diercks, O. M. Yaghi, *Science* **2017**, *355*, eaal1585.
[30] K. Geng, T. He, R. Liu, S. Dalapati, K. T. Tan, Z. Li, S. Tao, Y. Gong, Q. Jiang, D. Jiang, *Chem. Rev.* **2020**, *120*, 8814–8933.
[31] R. Liu, K. T. Tan, Y. Gong, Y. Chen, Z. Li, S. Xie, T. He, Z. Lu, H. Yang, D. Jiang, *Chem. Soc. Rev.* **2021**, *50*, 120–242.
[32] C. Zhang, B.-H. Wu, M.-Q. Ma, Z. Wang, Z.-K. Xu, *Chem. Soc. Rev.* **2019**, *48*, 3811–3841.
[33] H. Wang, M. Wang, X. Liang, J. Yuan, H. Yang, S. Wang, Y. Ren, H. Wu, F. Pan, Z. Jiang, *Chem. Soc. Rev.* **2021**, *50*, 5468–5516.
[34] F. Yang, J. Guo, C. Han, J. Huang, Z. Zhou, S.-P. Sun, Y. Zhang, L. Shao, *Sci. Adv.* **2024**, *10*, eadr9260.
[35] S. Kandambeth, A. Mallick, B. Lukose, M. V. Mane, T. Heine, R. Banerjee, *J. Am. Chem. Soc.* **2012**, *134*, 19524–19527.
[36] Z. Yang, Z.-W. Zhou, H. Guo, Z. Yao, X.-H. Ma, X. Song, S.-P. Feng, C. Y. Tang, *Environ. Sci. Technol.* **2018**, *52*, 9341–9349.
[37] Y. Zhang, J. Guo, G. Han, Y. Bai, Q. Ge, J. Ma, C. H. Lau, L. Shao, *Sci. Adv.* **2021**, *7*, eabe8706.
[38] Z. Zhang, X. Shi, Z. Zhang, B. Gao, L. Shao, Y. Wang, *Ind. Eng. Chem. Res.* **2024**, *63*, 14777–14785.
[39] Y. Shi, Z. Mai, Q. Shen, Q. Song, W. Fu, S. Xiang, M. Hu, K. Guan, R. Takagi, H. Matsuyama, *J. Membr. Sci.* **2024**, *702*, 122804.
[40] Z. Zhang, C. Yin, X. Shi, G. Yang, Y. Wang, *Sep. Purif. Technol.* **2022**, *283*, 120233.
[41] Q. Liu, M. Liu, Z. Zhang, C. Yin, J. Long, M. Wei, Y. Wang, *Nat. Commun.* **2024**, *15*, 9221.
[42] Z. Yang, P.-F. Sun, X. Li, B. Gan, L. Wang, X. Song, H.-D. Park, C. Y. Tang, *Environ. Sci. Technol.* **2020**, *54*, 15563–15583.
[43] Y. Qian, H. Li, J. Lu, D. Lu, H. Jin, Z. Xia, Z. Yao, J. Wang, L. Zhang, C. Y. Tang, *Environ. Sci. Technol.* **2023**, *57*, 10860–10869.
[44] F. Wang, Z. Yang, C. Y. Tang, *ACS ES&T Engineering* **2022**, *2*, 2023–2033.
[45] B. H. Gan, J. Gaynord, S. M. Rowe, T. Deingruber, D. R. Spring, *Chem. Soc. Rev.* **2021**, *50*, 7820–7880.
[46] P. Fang, W.-K. Pang, S. Xuan, W.-L. Chan, K. C.-F. Leung, *Chem. Soc. Rev.* **2024**, *53*, 11725–11771.
[47] C. Sgorbati, E. L.o Presti, G. Bergamaschi, M. Sani, A. Volonterio, *J. Org. Chem.* **2021**, *86*, 9225–9232.

Manuscript received: February 06, 2025
Revised manuscript received: April 15, 2025
Accepted manuscript online: May 06, 2025
Version of record online: ■■, ■■

Research Article

Porous Materials

B. Gao, Y. Gong, Z. Zhang*, Q. Liu, C. Yin, M. Wei, Y. Wang* — **e202503090**

Turing-Structured Covalent Organic Framework Membranes for Fast and Precise Peptide Separations

A Turing-structured COF membrane with externally striped and internally cavitated architectures is created via the modulation based on metal-polyphenol chemistry. The resulting COF membrane exhibits simultaneously enhanced water permeation and molecular sieving properties, demonstrating its great potential in the separation of high-value pharmaceuticals.